Electrons, Excitons and Hydrogen Bonding: Electron-promoted Desorption from Molecular Ice Surfaces

PCCP

Accepted Manuscript

This article can be cited before page numbers have been issued, to do this please use: D. Marchione and M. R. S. McCoustra, *Phys. Chem. Chem. Phys.*, 2016, DOI: 10.1039/C6CP05814K.

ROYAL SOCIETY OF CHEMISTRY

www.rsc.org/pccp

View Article Online
DOI: 10.1039/C6CP05814K

Journal Name

ARTICLE TYPE

Cite this: DOI: 10.1039/xxxxxxxxxx

Electrons, Excitons and Hydrogen Bonding: Electron-promoted Desorption from Molecular Ice Surfaces†

Demian Marchione*‡ and Martin R. S. McCoustra

Received Date
Accepted Date

DOI: 10.1039/xxxxxxxxxx

www.rsc.org/journalname

Desorption of benzene (C_6H_6) from thick methanol (CH_3OH) and diethyl ether ($CH_3CH_2OCH_2CH_3$) ices during irradiation with 250 eV electrons is reported and compared with our previous work on C_6H_6 desorption from water (H_2O) ice systems. C_6H_6 electron-promoted desorption (EPD) is seen to be sensitive to the chemical nature of the substrate reflecting both the importance of the excitations localised around the O-atom *versus* those involving the C-atom; and the role of hydrogen bonding interactions in transporting non-dissociative electronic excitation to the substrate/C_6H_6 interfaces during the electron irradiation.

1 Introduction

The physics and chemistry associated with irradiation of condensed phases by ionising radiation (*e.g.* ions, electrons, and energetic photons) is of considerable practical and fundamental interest. Photolysis and radiolysis of water (H_2O) vapour, aqueous solutions and thin films of H_2O have been thoroughly investigated in relation to their importance in radiation biology[1] and medicine[2] and in nuclear technology.[3–7] Solid water is also highly abundant in astrophysical environments: *e.g.* icy mantles coating interstellar dust grains;[8] and in icy bodies such as comets[9,10] and moons like Europa,[11,12] where exposure to ionising radiations is significant. Therefore, several laboratory studies have investigated the effect of electrons, ions and electromagnetic radiations on the physics and chemistry of H_2O ices highlighting what species are produced, by what mechanism these are formed, desorption of neutral or ionic species during the irradiation,[13–18] and phase changes.[19–22]

More recently, a great deal of attention has been given to better understanding the processes taking place after excitation by ionising radiation of other simple molecular solids containing species as methanol (CH_3OH), carbon monoxide (CO), acetonitrile (CH_3CN), ammonia (NH_3) at cryogenic temperatures.[23–33] The focus is usually on the chemistry in order to investigate the formation of complex organic molecules (COMs), including potential biogenic molecules, that have been detected in star and planet forming regions and likely originate from the evaporation of processed icy solids.[34–38] As illustrative, Mason and co-workers have presented results on 100 eV, 1 keV and 5 keV electron bombardment of thin CH_3OH films at 14 K.[39] The products and the yields seem to be similar regardless of the energy of the primary electrons suggesting that the observed electron-induced chemistry (EIC) is linked to lower energy, secondary excitations including electrons formed within the ice. The authors conclude with the hypothesis that these secondary excitations and electrons may represent a common progenitor in irradiation phenomena involving X-rays, cosmic rays and UV photons. This idea is supported by the work of Boamah *et al.*[25] which demonstrates that UV photon and low-energy ($\leq$ 20 eV) electron processing of methanol ices likely yield essentially the same reaction products.

Although much is known of the mechanisms by which these electrons are generated in the condensed phase,[40] there remain gaps in our knowledge specifically surrounding the role electronic excitations (excitons) and low energy electrons play in promoting physicochemical change especially in the interfacial or selvedge regions of the H_2O-rich environment.[41,42] In such regard, Akin *et al.*[43] have investigated the electron-stimulated desorption of molecular products from multilayer films of amorphous solid water (ASW) capped with sub-monolayer quantities of CH_3OH at 50 K. Their work demonstrated that EIC in H_2O films is quenched

Institute of Chemical Sciences, Heriot-Watt University, Edinburgh, EH14 4AS, UK. E-mail: marchionedemian@gmail.com, m.r.s.mccoustra@hw.ac.uk

† Electronic Supplementary Information (ESI) available: [details of any supplementary information available should be included here]. See DOI: 10.1039/b000000x/

‡ Present address: Science Division, Jet Propulsion Laboratory, California Institute of Technology, Pasadena, CA 91109, USA. Email:dmarchio@caltech.edu

View Article Online
DOI: 10.1039/C6CP05814K

by CH_3OH adlayers consistent with reactions occurring at the ASW/vacuum interface and not in the bulk of the film. The same group went on to present a thorough investigation of EIC in layered $H_2O/CO/H_2O$ ices;[44,45] changing the distance of the CO layer from the ASW/vacuum interface. In essence, the buried CO layer was used as a probe to disentangle the near surface processes from those characteristic of the bulk. They observed that hydrogenation reactions are dominant for more deeply buried CO layers, while oxidation is specific to the near-surface zone because of the low mobility of OH radicals.

In our previous work, we reported on the effect of low energy (100-350 eV) electrons on adlayers of benzene (C_6H_6) on solid H_2O surfaces observing a highly efficient desorption channel for loss of the aromatic species from the icy substrate upon irradiation.[46,47] In particular, it was found that efficient non-thermal desorption of C_6H_6 from solid H_2O is mediated by the icy underlayer *via* the formation of long-lived excitons in the H_2O bulk.[48] Then these diffuse to the H_2O/vacuum interface and hence C_6H_6/H_2O interface, promoting C_6H_6 desorption. Kinetically, the desorption behaviour is complex but typically exhibits two components; a fast component, with a cross-section up to 10^{-15} cm^2, and a slower component, with a cross-section of around 10^{-17} cm^2. The former is attributed to desorption of isolated C_6H_6 molecules hydrogen-bonded to small clusters of H_2O molecules on the solid water surface, while the latter is thought mainly to arise from desorption from larger C_6H_6 islands on the solid water surface. The key conclusions from this work are that the solid H_2O is necessary to observe the fast (*i.e.* 10^{-15} cm^2) C_6H_6 EPD channel and that the morphology of the C_6H_6/H_2O interface has a significant effect on the kinetics of such process.

Indirect desorption of this kind has been observed also for ices composed of volatile species such as CO, carbon dioxide (CO_2) or molecular nitrogen, N_2, during irradiation with VUV photons.[49,50] In essence, certain species can catalyse the non-thermal desorption of neighbouring molecules via excitation transfer through intermolecular bonds. This allows the so-called desorption induced by electronic transitions (DIET) mechanism to be operative and particularly relevant when the neighbouring compound would normally be transparent (read not active) in that excitation energy range.[51–53]

In this work, we continue our investigation of C_6H_6 EPD from icy substrates by irradiating with 250 eV electrons binary layered ices comprising of C_6H_6 on CH_3OH and C_6H_6 on diethyl ether ($CH_3CH_2OCH_2CH_3$) and compare the results to C_6H_6 on ASW. These systems were specifically chosen in order to allow us to elaborate on the role of hydrogen bonding in transporting the energy of secondary electronic excitations and its impact on desorption from the ice selvedge. Is excitation transport found only in solid H_2O? Is the excitation transport from the bulk to the interface linked to the type of intermolecular interactions that are established inside the bulk and at the interfaces of such systems? The series of experiments for C_6H_6 on top of H_2O, CH_3OH, and $CH_3CH_2OCH_2CH_3$ (chosen purely due to technical limitations in our experiment) layers strategically allows us to assess these open questions. In essence, we have reduced the degree of hydrogen bonding in the substrate film, and possibly between C_6H_6 and the substrate, by substituting the hydrogen atom (H) for an alkyl group, while retaining a consistent electronic excited states localised around the O-atom that might be responsible for the exciton formation and hence efficient C_6H_6 EPD.

2 Experimental

The experiments discussed here were performed in a stainless steel UHV chamber that has been described in detail elsewhere.[54,55] A combination of liquid-nitrogen-trapped diffusion pumps and a titanium sublimation pump allows to reach a base pressure in the chamber of $2 < 10^{-10}$ Torr at room temperature. The substrate is a polished stainless steel disk cooled by a liquid nitrogen in a reservoir in thermal contact with the sample mount giving a base temperature of 109 ± 2 K. The substrate was resistively heated up to 600 K for 15 minutes to remove volatile contaminants before cooling prior to conducting experiments each day. A K-type thermocouple, welded to the edge of the disk, was employed for temperature monitoring with a precision of 0.5 K.

Layered ices were obtained by sequential background deposition using C_6H_6 (Fluka 99.5% pure), de-ionised H_2O, CH_3OH (Sigma-Aldrich, HPLC grade 99.9% pure), or $CH_3CH_2OCH_2CH_3$ (Sigma-Aldrich, Chromasolv grade 99.9% pure). All the chemicals were stored in separate glass vials and were further purified by several freeze-pump-thaw cycles before use. Cross-contamination was avoided by collecting the vapour phase from the liquids using two independent manifolds each interfaced to its own dedicated fine-control leak valve (Vacuum Generators MD95). Exposure is reported in Langmuir units (1 L = 10^{-6} Torr s). Film thickness (d) can be estimated from:

$$d = \frac{SPt}{\sqrt{2\pi m k_B T}} \frac{1}{\rho_s} = \frac{Z_W t}{\rho_s} \quad (1)$$

S is the sticking coefficient assumed to be 1, P is the pressure recorded on the hot cathode ion gauge corrected for the approximate molecular ionisation efficiencies,[§ 56–59] t is the time of exposure, k_B is the Boltzmann constant, T is the temperature for the dosed molecules, Z_W is the bombardment rate (the incident flux), ρ_S is the molecular volume density and m is the mass. In the expression, we first define the number of molecules deposited onto the substrate (molecules per unit of surface area) during the dose and then divide this by the density (molecules per unit of volume).

§ 1.1 for H_2O, 1.87 for CH_3OH, 5.1 for $CH_3CH_2OCH_2CH_3$, and 6.0 for C_6H_6

View Article Online
DOI: 10.1039/C6CP05814K

Desorption of the species during the electron irradiation at 250 eV, was followed by a crossed-beam source, quadrupole mass spectrometer (VG Microtech PC300D, further modified by European Spectrometry Systems) with a homemade line-of-sight tube facing the front of the sample. Sample irradiation was performed using an electron gun (Kimball Physics, ELG-2) incident at *ca.* 30° with respect to the substrate normal and over an area of 1 mm^2. The resulting average electron flux was $(9 \pm 2) \times 10^{13}$ electron cm^{-2} s^{-1}, typically with a value of $(1.1 \pm 0.2) \times 10^{14}$ electron cm^{-2} s^{-1} in the first 50 s and quickly reaching a a limiting value of $(7.5 \pm 0.5) \times 10^{13}$ electron cm^{-2} s^{-1} at longer times.

The electron trajectories were simulated using the CASINO code.[60,61] Calculations for an electron beam at 250 eV, incident at 30°, consistent with the experimental conditions, showed that all the systems investigated the solid films have an overall larger thickness than the calculated electron maximum penetration depth. For example, assuming that the densities of the target molecular solids are 2.74×10^{22} molecule cm^{-3}, 1.91×10^{22} molecule cm^{-3}, 5.80×10^{21} molecule cm^{-3}, and 8.57×10^{21} molecule cm^{-3} for H_2O,[62–65] CH_3OH,[66] $CH_3CH_2OCH_2CH_3$¶, and C_6H_6[67] respectively, it is found for an energy of 250 eV that all of the incident electrons are stopped within the uppermost 7-9 nm of the ices. This is less than the thickness of the thinnest irradiated ice film (> 12 nm). Distributions of electrons within the film as a function of the ices depth are reported in the ESI.† However, the work of Barnett *et al.*[68] shows that the predicted electron penetration depths are significantly smaller than the experimentally observed electron damage depths at electron energies in the region ≤ 2 keV. It follows, we cannot rule out the possibility that especially for thinner films the primary electrons can travel through the entire ice. Therefore, in order to avoid the accretion of non-volatile carbonaceous material due to electron-induced chemistry at the metallic surface, we have used relatively large exposures of CH_3OH or $CH_3CH_2OCH_2CH_3$, respectively of 250 L and 500 L, for our EPD experiments. This approach has the additional advantage of neglecting any effect that the substrate could have during the irradiation.†

In order to semi-quantitatively discuss the change of primary ionisation depending on the intra-molecular structure, *ab initio* calculations were performed on simple model systems consisting of H_2O, CH_3OH, $CH_3CH_2OCH_2CH_3$. and the analogous cations (H_2O^+, CH_3OH^+, and $CH_3CH_2OCH_2CH_3^+$) using Gaussian 09[69] thanks to the EPSRC UK National Service for Computational Chemistry Software (NSCCS) at Imperial College London. All the systems were optimised, with no symmetry constrains, using the Møller-Plesset second order approach (MP2)[70,71] with a Dunning's augmented correlation-consistent polarised valance double-zeta basis set (aug-cc-pVDZ)[72–74] to estimate the HOMO-LUMO energy gap and the ionisation potential for the above mentioned species.

¶ Density of the liquid phase, Sigma-Aldrich

3 Results and Discussion

Previously we reported that the EPD behaviour of C_6H_6 on solid H_2O surfaces is dominated by two components: a prompt decay immediately following the onset of electron irradiation having a cross-section of $\sim 10^{-15}$ cm^2 and a slower decay with a cross-section of $\sim 10^{-17}$ cm^2.[46,47] The observed fast desorption can be schematically explained in terms of the following sequence of processes:

i Formation of secondary electrons in the H_2O film;

ii Primary and secondary electron scattering producing long-lived electronic excitations (excitons);

iii Migration of these excitons from the bulk to the C_6H_6/H_2O interface;

iv Excitation transfer from H_2O to the aromatic molecule via the π-hydrogen bond;

v C_6H_6 desorption.

Solid H_2O is a necessary substrate to observe efficient C_6H_6 EPD as the fast process is quenched at high C_6H_6 exposures when the H_2O film is completely covered by a C_6H_6 multilayer or is entirely absent when the substrate is amorphous silica. The nature of the C_6H_6/H_2O interface is also significant as it impacts on the intensity of the desorption trace and affects the kinetics of the slow component.[47]

Performing analogous measurements using solid CH_3OH and $CH_3CH_2OCH_2CH_3$ as substrates for the C_6H_6 provides the means to investigate the different steps of the mechanism above by highlighting the role of the hydrogen bonding in transferring the excitation both within the bulk and at the interface. The CH_3OH molecule can be regarded as being derived from H_2O following a substitution of one H-atom with a CH_3 group. Although the two species have similar electronic excitations localised on the O-atom, the insertion of a C-atom in the molecular structure adds a series of electronic states rich of C-character (see Fig. 1) which might impact the first two steps of the mechanism. Furthermore, the extent of the hydrogen-bonding network is significantly reduced in solid CH_3OH compared to H_2O, which might impact on exciton migration to the C_6H_6 interface (third step), if these form. According to the results presented in a previous work[75], the directed non-covalent interaction to the aromatic ring via the OH groups observed for C_6H_6/H_2O is still possible with CH_3OH substrate as for ASW (fourth step), although the CH_3 end also seem to accommodate the adsorption of C_6H_6. All these differences in the capability of the underlying ice to transmit the excitation

View Article Online
DOI: 10.1039/C6CP05814K

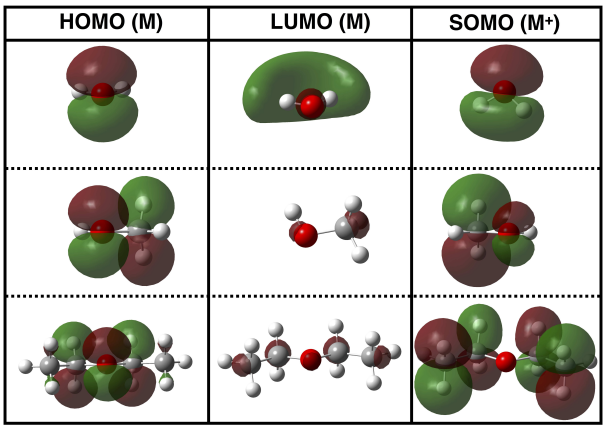

Fig. 1 Highest occupied and lowest unoccupied molecular orbitals for H_2O, CH_3OH, and $CH_3CH_2OCH_2CH_3$ and SOMOs for the analogous ions in the ground state. Iso-density value of $\pm$ 0.02 a.u. for the LUMO of the $CH_3CH_2OCH_2CH_3$, and $\pm$ 0.03 a.u. for all the others. Calculations were performed using MP2 approach with an aug-cc-pVDZ basis set. M represents the neutral molecule while M^+ is the corresponding cation.

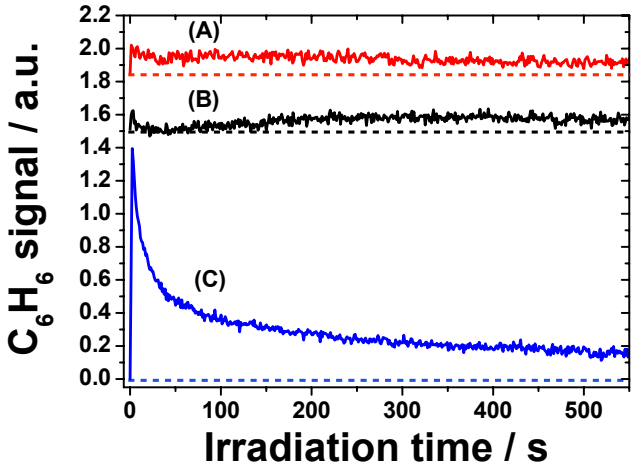

Fig. 2 C_6H_6 EPD signal obtained for 5 L of C_6H_6 on a thick ice of (A) $CH_3CH_2OCH_2CH_3$, in blue, (B) CH_3OH, in red, and (C) c-ASW, in black. Irradiation starts at t=0 s with 250 eV electrons. EPD traces have been offset for clarity with the dashed lines showing the zero lines for each curve.

and any possible implications arising from direct excitation of the C atom, are amplified when both H-atoms of the H_2O molecule are substituted with an aliphatic chain. In $CH_3CH_2OCH_2CH_3$ ice, chains of strong hydrogen bonded molecules are not present and interactions at the C_6H_6 interface are weaker than those established in the other two layered binary ices.

In this context, we have irradiated with 250 eV electrons the binary-layered ices of C_6H_6 pre-deposited on CH_3OH or on $CH_3CH_2OCH_2CH_3$. Fig. 2 compares the EPD traces corresponding to 5 L of C_6H_6 on a thick ice of c-ASW (100 L), CH_3OH (250 L), $CH_3CH_2OCH_2CH_3$ (500 L). It is noticeable that the intense signal observed for the desorbing C_6H_6 on solid H_2O substrate is decreased by at least an order of magnitude with respect to the other layered ices. In particular, in the C_6H_6/CH_3OH system, the initial fast desorption event can be assigned to a few aromatic molecules that are hydrogen-bonded to the substrate. The slowly rising tail can then be related to structural rearrangements within the underlayer, such as dangling OH formation, that slowly, but continuously, favour those conditions that determined the initial desorption. Furthermore, evidence from our structural study of these layered systems[75] suggests that the C_6H_6 "adlayer" would be similar on both c-ASW and on solid CH_3OH; presenting some isolated aromatic molecules which are hydrogen bonded to the substrate in between the islands of C_6H_6. By analogy between C_6H_6/H_2O and C_6H_6/CH_3OH, the second non-thermal desorption event might contain an additional contribution of the C_6H_6 leaving the surface of the C_6H_6 islands on the CH_3OH film. In contrast, the EPD trace from the $CH_3CH_2OCH_2CH_3$ substrate is somewhat reminiscent of the non-thermal desorption of C_6H_6 from thick C_6H_6 layers on c-ASW.[46,47]

In order to further elucidate the nature of the non-thermal desorption of C_6H_6 from the two thick CH_3OH and $CH_3CH_2OCH_2CH_3$ ices, we have performed electron irradiation experiments that investigate the dependence of the EPD signal as a function of the thickness of the C_6H_6 overlayer. Fig. 3 displays the results of this study. Despite the poor S/N ratio, two distinctive desorption events can be observed for both the datasets: a fast desorption, and a delayed, but long-lived and dominant component that immediately follows the former. These will be referred also as the *prompt* and the *dose dependent* C_6H_6 signals by analogy with the notation proposed by Kimmel and Petrik for the electron induced desorption of H_2 from ASW.[48] However, it is important to make a distinction: what we call dose dependent component in the C_6H_6 experiments increases with the surface coverage, while the trend is opposite for the dose dependent component of pure solid H_2O observed by Kimmel and co-workers since the mechanism for the two phenomena are likely to be unrelated.

A reasonable quantitative comparison between the prompt component and dose component for each EPD trace can be obtained in terms of the quantity, I_{prompt}/I_{dose}. This is the ratio of the intensities corresponding to the two contributions measured at the maximum while the other component can be assumed as negligible. The values of I_{prompt}/I_{dose} plotted as a function of C_6H_6 exposure are displayed in the upper panels of Fig. 4 and listed in Table 1. As C_6H_6 exposure is increased from 1 L to 5 L, the intensity ratio decreases to *ca.* 1 meaning that both prompt and

View Article Online
DOI: 10.1039/C6CP05814K

Table 1 List of values of intensity ratios and areas. The former is the ratio between the highest intensity of the prompt component, at t ∼ 0 s, over the maximum of the dose dependent component, generally between 200 s and 300 s. The values in square brackets refer to the C_6H_6 EPD from ASW in Fig. 2 and this was calculated as ratio between the intensities at t = 0 of the two components of the bi-exponential decay. Similarly, the I_{prompt}/I_{dose} ratio indicated in curly brackets corresponds to 50 L of C_6H_6 from ASW, irradiated with 300 eV electrons as reported in previous work.[46,47] The area under the C_6H_6 EPD curves is calculated by integration up to 600 s for different exposures of C_6H_6 on a thick CH_3OH or $CH_3CH_2OCH_2CH_3$ film. [a]Given the extremely low S/N ratio for the 1 L of C_6H_6 on CH_3OH, the area was calculated from integration of the smoothed curve and reported in brackets. The errors were estimated from the averaged uncertainty of the recorded intensity

C_6H_6 dose L	[CH_3OH] I_{prompt}/I_{dose}	[CH_3OH] Area / 10^{-11} a.u. s	[$CH_3CH_2OCH_2CH_3$] I_{prompt}/I_{dose}	[$CH_3CH_2OCH_2CH_3$] Area / 10^{-11} a.u. s
1	1.8 ± 0.9	$(1.0 \pm 0.5)^a$	2.0 ± 1.0	3.4 ± 1.7
5	1.1 ± 0.5 [2.05 ± 0.06]	2.5 ± 1.2	1.1 ± 0.4 [2.05 ± 0.06]	5.0 ± 1.8
10	0.40 ± 0.18	3.8 ± 1.7	0.50 ± 0.25	2.7 ± 1.3
20	0.40 ± 0.12	8.3 ± 2.5	0.50 ± 0.25	3.3 ± 1.6
50	0.50 ± 0.20 {1.8 ± 0.3}	5.2 ± 2.0	0.10 ± 0.05 {1.8 ± 0.3}	3.7 ± 1.8

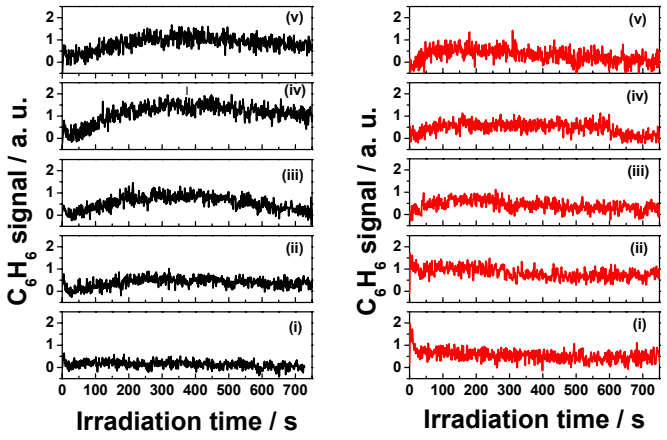

Fig. 3 The left panel shows the C_6H_6 EPD signal obtained for 1 L (i), 5 L (ii), 10 L (iii), 20 L (iv), and 50 L (v) of C_6H_6 on a thick CH_3OH film (18.9 nm), using black lines. The right panel displays the C_6H_6 EPD signal obtained for 1 L (i), 5 L (ii), 10 L (iii), 20 L (iv), and 50 L (v) of C_6H_6 on a thick $CH_3CH_2OCH_2CH_3$ film (30.2 nm) using red lines. Irradiation starts at t=0 s with 250 eV electrons. Note that the curves in this figure have been reported by dividing the C_6H_6 signal by a factor of one order of magnitude lower than that used in Fig. 2.

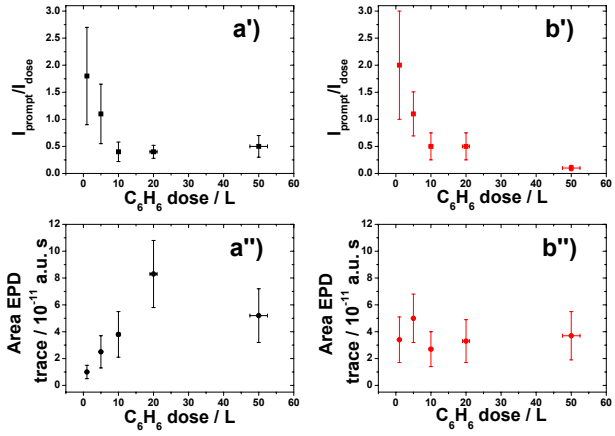

Fig. 4 The upper panels show the plots for I_{prompt}/I_{dose} ratio corresponding to each EPD trace as a function of C_6H_6 dose on the ices. The plots in the lower panels display how the total C_6H_6 yield (area up to 600 s) changes depending on the C_6H_6 coverage of the two substrates. The left panels, a′ and a″, refer to C_6H_6/CH_3OH while the right panels, b′ and b″, to $C_6H_6/CH_3CH_2OCH_2CH_3$. All data are taken from Table 1.

dose dependent components are equivalent to each other in the instant when these desorption events are most intense. By comparison, and as in Fig. 1, this ratio is *ca*. 2 for 5 L of C_6H_6 on ASW (Table 1) confirming that solid H_2O mediates a more efficient fast desorption of the aromatic adsorbate than the other two organic ices for the same C_6H_6 dose. As the C_6H_6 coverage on CH_3OH ices increases, I_{prompt}/I_{dose} reaches a plateau around 0.5 while this decreases down to 0.1 for $CH_3CH_2OCH_2CH_3$ ices. In conclusion the prompt desorption is negligible for both systems at C_6H_6 exposures ≥10 L, while this is more important at lower exposures, *e.g.* 1 L and 5 L. However, it should be stressed that in the latter cases the I_{prompt}/I_{dose} ratio is relatively high mainly because the C_6H_6 dose is too low to result in a significant contribution to the slow desorption component. In fact, as displayed in Fig. 3, the absolute intensity of the EPD traces is rather small, including in the first instants of irradiation when the prompt desorption is most relevant.

Focusing on the dose dependent component for C_6H_6/CH_3OH as displayed in Fig. 3, the signal grows in intensity as more molecules are deposited onto the ice, with the only exception being the 50 L EPD trace that seems to reverse this trend. Such behaviour was proved to be reproducible, and hence cannot be attributed to random fluctuations in the recorded signal. A confirmation to the described trend can be obtained by comparing the areas underlying each of the EPD curves up to 600 s as listed

View Article Online
DOI: 10.1039/C6CP05814K

in Table 1 and plotted in the upper left panel of Fig. 4. In fact, for both the layered ices the prompt component (integration up to *ca.* 20 s) accounts for 0 - 4% of the total signal (integration up to 600 s). Therefore, the trend observed for the total area, gross C_6H_6 desorption yield, as a function of C_6H_6 dose is modulated by the change in the dose dependent component. As reported in Table 1 and in the left lower panel of Fig. 4, the total area for C_6H_6/CH_3OH, grows almost linearly from 1 L to 20 L, where this is largest, and then decreases at 50 L.

The quality of the signal is extremely poor also for the analogous data set from the $C_6H_6/CH_3CH_2OCH_2CH_3$ system as shown in Fig. 3 (right panel). There is a clear evidence of the prompt event disappearing at larger exposures since this accounts for the 8% of the total signal at 1 L of C_6H_6 and 0% above 10 L while I_{prompt}/I_{dose} decreases of 20 times. Therefore, the dose dependent component is the dominant process of the observed electron-promoted desorption. Furthermore, the EPD signal associated to the 20 L experiment drops suddenly at 600 s, while the decay is more gentle for 10 L and 50 L of C_6H_6. Repeating the experiment confirmed this unusual behaviour that, hence, must be linked to an actual process occurring in the ice during the irradiation. Details of this are still unclear, but it could be related to erosion and changes in both the film structure and composition due to the electron processing.

In contrast with C_6H_6/CH_3OH, the integration of the EPD curves for $C_6H_6/CH_3CH_2OCH_2CH_3$ gives similar values over the entire range of C_6H_6 exposures explored as Table 1 and the right lower panels of Fig. 4 show. The observed trends for the two desorption components between the layered ices are consistent with a distinct mechanism of the C_6H_6 film growth on CH_3OH and on $CH_3CH_2OCH_2CH_3$ substrates. A combination of *ab initio* calculations, and TPD and RAIR experiments performed on these systems[75] indicates that the C_6H_6 adlayer wets the $CH_3CH_2OCH_2CH_3$ surface. Hence, at 1 L, all the underlying ice would be almost completely covered by the adsorbate. Therefore, this could maximize any electron promoted-desorption mediated by the upper layer of the $CH_3CH_2OCH_2CH_3$ ice. It is not clear whether this mechanism involves energy transfer following the excitation of the O-atoms or the exothermicity associated to electron-induced reactions at the interface and further studies are required. At higher exposures, certainly above 10 L, the outer C_6H_6 layers might act as a cap, preventing the molecules at the interface below from desorbing. Thus only the characteristic EPD of C_6H_6 multi-layers is detected while the substrate-mediated mechanism is quenched. Moreover, the relatively higher value of area corresponding to the 5 L EPD curve (see Table 1, lower right panel in Fig. 4) might be symptomatic of a transition of regimes from EPD mediated by the substrate to direct EPD of C_6H_6. However, the overall insensitivity of C_6H_6 desorption yield as a function of the coverage is consistent with a layer-by-layer growth mechanism.

In contrast, C_6H_6 does not completely wet the CH_3OH ice, and thus larger exposures are required to "fill the gaps" between the C_6H_6 islands. This means that the prompt event is detected also at large C_6H_6 exposures, explaining why the I_{prompt}/I_{dose} ratio is 0.5 also at 50 L and does not go to lower values (*e.g. 0.1*) as it happens for C_6H_6 on $CH_3CH_2OCH_2CH_3$. This behaviour is not dissimilar to that reported by Thrower for 50 L of C_6H_6 on ASW[46,47] irradiated with 300 eV electrons resulting in a I_{prompt}/I_{dose} ratio of 1.8 ± 0.3. A further insight into the relationship between the C_6H_6 growth mechanism and the way the desorption yield changes with the adlayer coverage (Fig. 4) can be inferred by focusing on the dose dependent component. This might potentially contain several contributions: 1) physicochemical changes within the substrate such as chemical reactions and reorientation at the CH_3OH/vacuum interface, 2) multilayer C_6H_6 desorption, and 3) non-thermal diffusion from the island edges to the CH_3OH/vacuum interface. For the range of C_6H_6 exposures probed, the islands on CH_3OH would become progressively bigger. It follows that the more molecules are available, the more long-lived is the EPD (*e.g.* 5 - 20 L traces in the left panel of Fig. 3); and hence the repopulation of the "active" sites at the ice interface should in principle be enhanced too. At 50 L, the gaps between the islands would be almost filled, quenching the contribution given by the CH_3OH surface to the slow component. This would explain why on CH_3OH the 20 L trace has a more marked bump (larger area) than the 50 L data (Fig. 4, panel a$''$).

4 Effect of Intermolecular Forces on Exciton Transport

To summarise, as the poor S/N ratio of our experiments illustrate, EPD of C_6H_6 is efficient from ASW surfaces, while is negligible from the CH_3OH and $CH_3CH_2OCH_2CH_3$ substrates. The former case results from the combination of two features of solid H_2O:

i The electronic excitations of the O-atom lying in the 21-8.7 eV range[14,76,77] are compatible with the energy distribution of the secondary electrons produced during the irradiation resulting in the formation of excitons in the ASW film;

ii The extended three-dimensionality of the hydrogen bonding network within ASW that allows both transportation of excitons over large distances (potentially 10s of nm) from the bulk to the interface, and excitation transfer to the aromatic ring *via* dangling OH groups or *via* exciton relaxation and excitation of the π-hydrogen bond followed by desorption.

In contrast, for CH_3OH and $CH_3CH_2OCH_2CH_3$ the chemistry of C-atom becomes relevant. Fig. 1 shows that the highest occupied molecular orbital (HOMO) and the lowest unoccupied molecular orbital (LUMO) for gas-phase H_2O, CH_3OH and

View Article Online
DOI: 10.1039/C6CP05814K

$CH_3CH_2OCH_2CH_3$ along with the semi-occupied molecular orbital (SOMO) of their analogous cations. The substitution of the H-atoms with aliphatic groups does not significantly alter the electron density around the oxygen atoms in the HOMOs for the neutral species. However, this substitution introduces molecular orbital components around the C atoms. More evidently, going from H_2O to CH_3OH and to $CH_3CH_2OCH_2CH_3$, the LUMOs and the SOMOs display less and less oxygen character, opening different routes for relaxation. Table 2 reports the HOMO-LUMO gap, ΔE_1, and the ionisation potential, ΔE_2 for each species. The latter was calculated as energy difference between the cation and the corresponding neutral molecule. Both terms decrease as the

Table 2 List of values in eV of the HOMO-LUMO energy gap (ΔE_1) and of the ionisation potential (ΔE_2) for H_2O, CH_3OH or $CH_3CH_2OCH_2CH_3$. Calculations were performed using MP2 approach with an aug-cc-pVDZ basis set

Molecule	ΔE_1/eV	ΔE_2/eV
H_2O	14.8 eV	12.6 eV
CH_3OH	13.2 eV	11.1 eV
$CH_3CH_2OCH_2CH_3$	12.4 eV	9.9 eV

H-atoms are substituted with alkyl groups, thus, both ionisation and excitation become more energetically accessible as the final state becomes richer in C-atom character. A quantitative and detailed description of the lowest excitations and ionisations for these molecules is beyond the scope of the present work. Obviously, ground state MP2 calculations on gas phase molecules fail to accurately model the band energies in solid H_2O, CH_3OH, and $CH_3CH_2OCH_2CH_3$, but provide visual and logically sound evidence for the potential relevance of C-atom chemistry that might involve excitations in the 8.4 -11.6 eV range.[78,79] For instance, all electronic excited states of methane (CH_4) are dissociative[80] including the lowest lying ones, which have theoretical thresholds of 10-12 eV.[81] These values are also compatible with the energy distribution of the secondary electrons formed in our experiments supporting the idea that the C-atom chemistry is relevant for organic ices. In fact, irradiation experiments of pure methane (CH_4) ices with 5 keV electrons at 10 K[82] show that the predominant reaction pathway is the homolytic cleavage of the C-H bond. Then H-atoms recombine to form molecular hydrogen which was the sole species detected in gas-phase during the irradiation. Recombination of methyl fragments (CH_3) generates internally excited ethane molecules that can undergo additional dehydrogenation steps too. Future work will investigate the relevance of H_2 formation and subsequent desorption in ices comprised of organic molecules.

However, we should stress that in condensed phases, especially solids, the coupling with the neighbouring molecules might establish a barrier that is sufficient to support a quasi-bound vibrational states even for those excited states which are purely dissociative in gas phase. This has been proposed for condensed H_2O phases[83] where the excited state lifetime might be long enough for exciton migration, providing a mechanism for energy transport. In other words, the stronger the intermolecular interaction is the more effective the coupling is between the excited molecule and the surrounding environment, enhancing the probability for excitation transfer. The 3-dimensionality of hydrogen bonding network in solid H_2O allows for exciton migration across several layers, from the bulk to the vacuum interface.[48,84]

Elkins *et al.* have investigated the charge-transfer-to-solvent dynamics and excited state relaxation mechanism of solvated electron in a liquid CH_3OH microjet by means of two-pulse and three-pulse experiments.[85] The authors observe that CH_3OH shows identical excited state dynamics to H_2O. Therefore, for solid CH_3OH and perhaps for $CH_3CH_2OCH_2CH_3$, the weaker hydrogen bonding interactions might result in inefficient excitation transfer although it remains possible. Therefore, assuming that O-localised excitations were to be not negligible in CH_3OH (and $CH_3CH_2OCH_2CH_3$) ices, these would possibly lead to exciton formation somehow, especially in light of the fact that intermolecular forces are mostly directed towards the O-atom, and could potentially allow the formation of quasi-bound states. These would mediate transportation of the excitation energy, from molecule to molecule, to the interface although the significant reduction of (or absence of) a hydrogen bonding network within the solid with respect to ASW will severely hinder exciton migration and perhaps encourage exciton relaxation and hence fragmentation.[86,87] This is consistent with our results in Fig. 3 that displays a very low, but detectable, signal for the EPD of C_6H_6 from both CH_3OH and $CH_3CH_2OCH_2CH_3$ surfaces compared to ASW substrates.

5 Conclusions

Electron irradiation experiments confirm that solid H_2O is a necessary substrate to observe efficient desorption of C_6H_6, which can be interpreted in terms of exciton formation and migration to the interface as proposed by Kimmel and co-workers for H_2 formation in solid H_2O.[48] Furthermore, we have demonstrated that this mechanism is significantly quenched in CH_3OH and $CH_3CH_2OCH_2CH_3$ ices. The fact that the prompt desorption is less intense in the absence of H_2O is rather noticeable when taking into account the similarities between the C_6H_6/CH_3OH and C_6H_6/ASW ices. This change in the EPD process is likely linked to:

- The decreased extent of the hydrogen-bonding network that limits the propagation of excitons from the bulk to the interface meaning that only the outer CH_3OH layers could promote the C_6H_6 desorption efficiently.

- Exciton formation might not occur at all in the solid CH_3OH because primary and secondary electrons stimulate C-atoms

View Article Online
DOI: 10.1039/C6CP05814K

instead of O-atoms, favouring chemistry over physical processes such as desorption. In other words, the substitution of the H atom with a methyl (CH_3) group introduces an additional electron rich centre capable of being excited by the incident, primary and secondary, electrons. While H_2O has the electron density markedly centred at the O-atom, the C-atom in CH_3OH carries an additional spectrum of electronic excitation that might favour other processes over desorption. This is probably amplified in the case of the $CH_3CH_2OCH_2CH_3$ ice, where each molecule has four carbon atoms, against one oxygen, that are capable of channelling the secondary electron energies towards reactive routes.[81,82,88–91]

- EPD of C_6H_6 from CH_3OH and $CH_3CH_2OCH_2CH_3$ ices is still observed. Although this is a rather minor process, more so in $CH_3CH_2OCH_2CH_3$ than in CH_3OH, both a prompt and a dose-dependent component are noted. The latter correlates with the surface coverage of C_6H_6, while the former, barely visible, is consistent with substrate-mediated desorption via a mechanism yet to be clarified.

To conclude, in a previous work we have highlighted the relevance of the efficient EPD from ASW surfaces in astrophysical contexts[47] and the same can be briefly done for the EPD experiments here presented. In fact, since the icy mantles of the ISM dust grains is mainly made of H_2O, non-thermal desorption of small molecules bound to the ice surface via a dangling OH group can slow the formation of complex organic molecules (COM) on the surfaces of grains themselves. On the basis of the new results, we conclude that once the hydrogenation of CO leads to a sufficient mantle enrichment of CH_3OH and other organic molecules, the EPD process will no longer be important, and, in contrast, electron-induced synthesis will boost the accretion of COMs.

6 Acknowledgments

The authors would like to acknowledge the use of the EPSRC UK National Service for Computational Chemistry Software (NSCCS) at Imperial College London and contributions from its staff in carrying out this work. The authors acknowledge the support of the European Community FP7-ITN Marie-Curie Programme (LASSIE project, grant agreement #238258). Financial support from Heriot-Watt University for a number of upgrades to the UHV system is also acknowledged. DM clarifies that his contribution to this work has been done as a private venture and not in the author's capacity as an affiliate of the Jet Propulsion Laboratory, California Institute of Technology.

References

1 B. Boudaïffa, P. Cloutier, D. Hunting, M. A. Huels and L. Sanche, *Science*, 2000, **287**, 1658–1660.
2 Y. Hatano, Y. Katsumura and A. Mozumder, *Charged Particles and Photon Interactions with Matter; Mozumder*, CRC Press, Boca Raton, FL, 2010.
3 G. S. Was, Y. Ashida and P. L. Andresen, *Corros. Rev.*, 2011, **29**, 7–49.
4 A. Garibov, *Nukleonika*, 2011, **56**, 333–342.
5 A. G. Chmielewski, *Nukleonika*, 2011, **56**, 241–249.
6 K. Ishigure, Y. Katsumura, G. R. Sunaryo and D. Hiroishi, *Radiat. Phys. Chem.*, 1995, **46**, 557–560.
7 H. Christensen, *Radiat. Phys. Chem.*, 1981, **18**, 147–158.
8 K. I. Öberg, A. C. A. Boogert, K. M. Pontoppidan, S. van den Broek, E. F. van Dishoeck, B. Sandrine, A. B. Geoffrey and N. J. Evans II, *Astrophys. J.*, 2011, **740**, 109.
9 H. Balsiger, K. Altwegg and J. Geiss, *J. Geophys. Res.*, 1995, **100**, 5827–5834.
10 K. Altwegg, H. Balsiger, A. Bar-Nun, J. J. Berthelier, A. Bieler, P. Bochsler, C. Briois, U. Calmonte, M. Combi, J. De Keyser, P. Eberhardt, B. Fiethe, S. Fuselier, S. Gasc, T. I. Gombosi, K. Hansen, M. Hässig, A. Jäckel, E. Kopp, A. Korth, L. LeRoy, U. Mall, B. Marty, O. Mousis, E. Neefs, T. Owen, H. Rème, M. Rubin, T. Sémon, C.-Y. Tzou, H. Waite and P. Wurz, *Science*, 2015, **347**, 1–6.
11 M. S. Gudipati and J. Castillo-Rogez, *The Science of Solar System Ices*, Springer, USA, 2013.
12 C. J. Bennett, C. Pirim and T. M. Orlando, *Chem. Rev.*, 2013, **113**, 9086–9150.
13 P. Rowntree, L. Parenteau and L. Sanche, *J. Chem. Phys.*, 1991, **94**, 8570–8576.
14 G. A. Kimmel, T. M. Orlando, C. Vézina and L. Sanche, *J. Chem. Phys.*, 1994, **101**, 3282–3286.
15 N. G. Petrik and G. A. Kimmel, *J. Chem. Phys.*, 2005, **123**, 054702.
16 N. G. Petrik, A. G. Kavetsky and G. A. Kimmel, *J. Chem. Phys.*, 2006, **125**, 124702.
17 T. M. Orlando and G. A. Kimmel, *Surf. Sci.*, 1997, **390**, 79–85.
18 W. Zheng, D. Jewitt and R. I. Kaiser, *Astrophys. J.*, 2006, **639**, 534–548.
19 M. H. Moore and R. L. Hudson, *Astrophys. J.*, 1992, **401**, 353–360.
20 G. Strazzulla, G. A. Baratta, G. Leto and G. Foti, *Europhys. Lett.*, 1992, **18**, 517–522.
21 W. Zheng, D. Jewitt and R. I. Kaiser, *J. Phys, Chem. A*, 2009, **113**, 11174–11181.
22 G. Leto and G. A. Baratta, *Astron. Astrophys.*, 2003, **397**, 7–13.
23 S. Maity, R. I. Kaiser and B. M. Jones, *Faraday Discuss.*, 2014, **168**, 485–516.
24 S. Maity, R. I. Kaiser and B. M. Jones, *Phys. Chem. Chem. Phys.*, 2015, **17**, 3081–3114.

View Article Online
DOI: 10.1039/C6CP05814K

25 M. D. Boamah, K. K. Sullivan, K. E. Shulenberger, C. M. Soe, L. M. Jacob, F. C. Yhee, K. E. Atkinson, M. C. Boyer, D. R. Haines and C. R. Arumainayagam, *Faraday Discuss.*, 2014, **168**, 249–266.

26 A. G. M. Abdulgalil, D. Marchione, A. Rosu-Finsen, M. P. Collings and M. R. S. McCoustra, *J. Vac. Sci. Technol. A*, 2012, **30**, 0415051.

27 A. G. M. Abdulgalil, D. Marchione, J. D. Thrower, M. P. Collings, M. R. S. McCoustra, I. F., M. E. Palumbo, E. Congiu and F. Dulieu, *Phil. Trans. R. Soc. A*, 2013, **371**, 20110586.

28 F. de A. Ribeiro, G. C. Almeida, Y. Garcia-Basabe, W. Wolff, H. M. Boechat-Roberty and M. L. M. Rocco, *Phys. Chem. Chem. Phys.*, 2015, **17**, 27473–27480.

29 W. Zheng and R. I. Kaiser, *J. Phys. Chem. A*, 2010, **114**, 5251–5255.

30 H. M. Moore, R. F. Ferrante, R. L. Hudson and J. N. Stone, *Icarus*, 2007, **190**, 260–273.

31 B. L. Henderson and M. S. Gudipati, *Astrophys. J.*, 2015, **800**, 66.

32 S. Jheeta, A. Domaracka, S. Ptasinska, B. Sivaraman and N. J. Mason, *Chem. Phys. Lett.*, 2013, **556**, 359–364.

33 K. K. Sullivan, M. D. Boamah, K. E. Shulenberger, S. Chapman, K. E. Atkinson, M. C. Boyer and C. R. Arumainayagam, *Mon. Not. R. Astron. Soc.*, 2016, **460**, 664–672.

34 E. Herbst and E. F. van Dishoeck, *Ann. Rev. Astron. Astrophys.*, 2009, **47**, 427–480.

35 N. Sakai, C. Ceccarelli, S. Bottinelli, T. Sakai and S. Yamamoto, *Astrophys. J.*, 2012, **754**, 70.

36 E. Caux, C. Kahane, A. Castets, A. Coutens, C. Ceccarelli, A. Bacmann, S. Bisschop, S. Bottinelli, C. Comito, F. P. Helmich, B. Lefloch, B. Parise, P. Schilke, A. G. G. M. Tielens, E. van Dishoeck, C. Vastel, V. Wakelam and A. Walters, *Astron. Astrophys.*, 2011, **532**, A23.

37 T. Henning and D. Semenov, *Chem. Rev.*, 2013, **113**, 9016–9042.

38 K. I. Öberg, E. C. Fayolle, J. B. Reiter and C. Cyganowski, *Faraday Discuss.*, 2014, **168**, 81–101.

39 N. J. Mason, B. Nair, S. Jheeta and E. Szymanska, *Faraday Discuss.*, 2014, **168**, 235–247.

40 J. Savolainen, F. Uhlig, S. Ahmed, P. Hamm, and P. Jungwirth, *Nature*, 2014, **6**, 697–701.

41 B. C. Garrett, D. A. Dixon, D. M. Camaioni, D. M. Chipman, M. A. Johnson, C. D. Jonah, G. A. Kimmel, J. H. Miller, T. N. Rescigno, P. J. Rossky, S. S. Xantheas, S. D. Colson, A. H. Laufer, D. Ray, P. F. Barbara, D. M. Bartels, K. H. Becker, K. H. Bowen, S. E. Bradforth, I. Carmichael, J. V. Coe, L. R. Corrales, J. P. Cowin, M. Dupuis, K. B. Eisenthal, J. A. Franz, M. S. Gutowski, K. D. Jordan, B. D. Kay, J. A. LaVerne, S. V. Lymar, T. E. Madey, C. W. McCurdy, D. Meisel, S. Mukamel, A. R. Nilsson, T. M. Orlando, N. G. Petrik, S. M. Pimblott, J. R. Rustad, G. K. Schenter, S. J. Singer, A. Tokmakoff, L.-S. Wang and T. S. Zwier, *Chem. Rev.*, 2005, **105**, 355–390.

42 E. Alizadeh and L. Sanche, *Chem. Rev.*, 2012, **112**, 5578–5602.

43 M. C. Akin, N. G. Petrik and G. A. Kimmel, *J. Chem. Phys.*, 2009, **130**, 104710.

44 N. G. Petrik, R. J. Monckton, S. P. K. Koehler and G. A. Kimmel, *J. Chem. Phys.*, 2014, **140**, 204710.

45 N. G. Petrik, R. J. Monckton, S. P. K. Koehler and G. A. Kimmel, *J. Phys. Chem. C*, 2014, **118**, 27483–27492.

46 J. D. Thrower, M. P. Collings, F. J. M. Rutten and M. R. S. McCoustra, *Chem. Phys. Lett.*, 2011, **505**, 106–111.

47 D. Marchione, J. D. Thrower and M. R. S. McCoustra, *Phys. Chem. Chem. Phys.*, 2016, **18**, 4026–4034.

48 N. G. Petrik and G. A. Kimmel, *Phys. Rev. Lett.*, 2003, **90**, 166102.

49 J.-H. Fillion, E. C. Fayolle, X. Michaut, M. Doronin, L. Philippe, J. Rakovsky, C. Romanzin, N. Champion, K. I. Oberg, H. Linnartz and M. Bertin, *Faraday Discuss.*, 2014, **168**, 533–552.

50 Martín-Doménech, R., Manzano-Santamaría, J., Muñoz Caro, G. M., Cruz-Díaz, G. A., Chen, Y.-J., Herrero, V. J. and Tanarro, I., *Astron. Astrophys.*, 2015, **584**, A14.

51 J. D. Thrower, D. J. Burke, M. P. Collings, A. Dawes, P. D. Holtom, F. Jamme, P. Kendall, W. A. Brown, I. P. Clark, H. J. Fraser, M. R. S. McCoustra, N. J. Mason and A. W. Parker, *Astrophys. J.*, 2008, **673**, 1233–1239.

52 J. D. Thrower, D. J. Burke, M. P. Collings, A. Dawes, P. D. Holtom, F. Jamme, P. Kendall, W. A. Brown, I. P. Clark, H. J. Fraser, M. R. S. McCoustra, N. J. Mason and A. W. Parker, *J. Vac. Sci. Technol. A*, 2008, **26**, 919–924.

53 J.-H. Fillion, *Faraday Discuss.*, 2014, **168**, 423–448.

54 J. D. Thrower, M. P. Collings, F. J. M. Rutten and M. R. S. McCoustra, *Mon. Not. R. Astron. Soc.*, 2009, **394**, 1510–1518.

55 J. D. Thrower, M. P. Collings, F. J. M. Rutten and M. R. S. McCoustra, *J. Chem. Phys.*, 2009, **131**, 244711.

56 R. L. Summers, *Empirical observations on the sensitivity of hot cathode ionization type vacuum gauges*, National Aeronautics and Space Administration, Washington, D. C., 1969.

57 J. E. Bartmess and M. Georgiadis, R, *Vacuum*, 1983, **33**, 149-153.

58 M. Schulte, B. Schlosser and W. Seidel, *Fresenius J. Anal. Chem.*, 1994, **348**, 778–780.

59 G. D. Waddill and L. L. Kesmodel, *Phys. Rev. B*, 1985, **31**, 4940–4946.

60 P. Hovington, D. Drouin and R. Gauvin, *Scanning*, 1997, **19**, 1–14.

61 D. Drouin, A. R. Couture, D. Joly, X. Tastet, V. Aimez and

View Article Online
DOI: 10.1039/C6CP05814K

R. Gauvin, *Scanning*, 2007, **29**, 92–101.

62 G. A. Kimmel, Z. Dohnálek, K. P. Stevenson, R. S. Smith and B. D. Kay, *J. Chem. Phys.*, 2001, **114**, 5295–5303.

63 G. A. Kimmel, K. P. Stevenson, R. S. Smith and B. D. Kay, *J. Chem. Phys.*, 2001, **114**, 5284–5294.

64 M. S. Westley, G. A. Baratta and R. A. Baragiola, *J. Chem. Phys.*, 1998, **108**, 3321–3326.

65 D. E. Brown, , S. M. George, C. Huang, E. K. L. Wong, K. B. Rider, R. S. Smith, and B. D. Kay, *J. Phys. Chem.*, 1996, **100**, 4988–4995.

66 S. D. Green, A. S. Bolina, R. Chen, M. P. Collings, W. A. Brown and M. R. S. McCoustra, *Mon. Not. R. Astron. Soc.*, 2009, **398**, 357–367.

67 C. J. Craven, P. D. Hatton, C. J. Howard and G. S. Pawley, *J. Chem. Phys.*, 1993, **98**, 8236–8243.

68 I. L. Barnett, A. Lignell and M. S. Gudipati, *Astrophys. J.*, 2012, **747**, 13.

69 M. J. Frisch, G. W. Trucks, H. B. Schlegel, G. E. Scuseria, M. A. Robb, J. R. Cheeseman, G. Scalmani, V. Barone, B. Mennucci, G. A. Petersson, H. Nakatsuji, M. Caricato, X. Li, H. P. Hratchian, A. F. Izmaylov, J. Bloino, G. Zheng, J. L. Sonnenberg, M. Hada, M. Ehara, K. Toyota, R. Fukuda, J. Hasegawa, M. Ishida, T. Nakajima, Y. Honda, O. Kitao, H. Nakai, T. Vreven, J. A. Montgomery, Jr., J. E. Peralta, F. Ogliaro, M. Bearpark, J. J. Heyd, E. Brothers, K. N. Kudin, V. N. Staroverov, R. Kobayashi, J. Normand, K. Raghavachari, A. Rendell, J. C. Burant, S. S. Iyengar, J. Tomasi, M. Cossi, N. Rega, J. M. Millam, M. Klene, J. E. Knox, J. B. Cross, V. Bakken, C. Adamo, J. Jaramillo, R. Gomperts, R. E. Stratmann, O. Yazyev, A. J. Austin, R. Cammi, C. Pomelli, J. W. Ochterski, R. L. Martin, K. Morokuma, V. G. Zakrzewski, G. A. Voth, P. Salvador, J. J. Dannenberg, S. Dapprich, A. D. Daniels, Ã. Farkas, J. B. Foresman, J. V. Ortiz, J. Cioslowski and D. J. Fox, *Gaussian09 Revision D.01*, Gaussian Inc. Wallingford CT 2009.

70 C. Møller and M. S. Plesset, *Phys. Rev.*, 1934, **46**, 618–622.

71 M. Head-Gordon, J. A. Pople and M. J. Frisch, *Chem. Phys. Lett.*, 1988, **153**, 503–506.

72 T. H. Dunning, *J. Chem. Phys.*, 1989, **90**, 1007–1023.

73 R. A. Kendall, T. H. Dunning and R. J. Harrison, *J. Chem. Phys.*, 1992, **96**, 6796–6806.

74 D. E. Woon and T. H. Dunning, *J. Chem. Phys.*, 1993, **98**, 1358–1371.

75 D. Marchione and M. R. S. McCoustra, *Phys. Chem. Chem. Phys.*, 2016, **18**, 20790–20801.

76 C. D. Wilson, C. A. Dukes and R. A. Baragiola, *Phys. Rev. B*, 2001, **63**, 121101.

77 K. Kobayashi, *J. Phys. Chem.*, 1983, **87**, 4317–4321.

78 G. A. Cruz-Diaz, G. M. M. n. Caro and Y.-J. Chen, *Mon. Not. R. Astron. Soc.*, 2014, **439**, 2370–2376.

79 Y.-P. Kuo, H.-C. Lu, Y.-J. Wu, B.-M. Cheng and J. F. Ogilvie, 2007, **447**, 168–174.

80 G. Herzberg, *Molecular Spectra and Molecular Structure III. Electronic Spectra of Polyatomic Molecules*, Van Nostrand Reinhold, New York, 1966.

81 C. Winstead, Q. Sun, V. McKoy, J. L. S. Lino and M. A. P. Lima, *J. Chem. Phys.*, 1993, **98**, 2132–2137.

82 C. J. Bennett, C. S. Jamieson, Y. Osamura and R. I. Kaiser, *Astrophys. J.*, 2006, **653**, 792–811.

83 D. M. Chipman, *J. Chem. Phys.*, 2006, **124**, 044305.

84 N. G. Petrik and G. A. Kimmel, *J. Chem. Phys.*, 2004, **121**, 3727–3735.

85 M. H. Elkins, H. L. Williams and D. M. Neumark, *J. Chem. Phys.*, 2015, **142**, 234501.

86 D. Marchione, *PhD thesis*, Heriot-Watt University, 2015.

87 D. Marchione and M. R. S. McCoustra, *in preparation*.

88 M. C. Boyer, M. D. Boamah, K. K. Sullivan, C. R. Arumainayagam, M. Bazin, A. D. Bass and L. Sanche, *J. Phys. Chem. C*, 2014, **118**, 22592–22600.

89 R. I. Kaiser, S. Maity and B. M. Jones, *Phys. Chem. Chem. Phys.*, 2014, **16**, 3399–3424.

90 M. Kitajima, R. Suzuki, K. Otoguro, T. Ishihara and H. Tanaka, *Phys. Scripta*, 2004, **T110**, 420–423.

91 A. Wada, N. Mochizuki and K. Hiraoka, *Astrophys. J.*, 2006, **644**, 300–306.